

Activated carbon-hybridized and amine-modified polyacrylonitrile nanofibers toward ultrahigh and recyclable metal ion and dye adsorption from wastewater

Fengli Li¹, Chuang Chen¹, Yuda Wang¹, Wenpeng Li¹, Guoli Zhou (✉)¹, Haoqin Zhang¹,
Jie Zhang (✉)¹, Jingtao Wang^{1,2}

¹ School of Chemical Engineering, Zhengzhou University, Zhengzhou 450001, China

² Henan Institute of Advanced Technology, Zhengzhou University, Zhengzhou 450003, China

© Higher Education Press 2021

Abstract Nanofibers with high specific surface area and chemical stability have broad prospects in the applications of adsorption. However, the adsorption capacity is limited by the scarcity of adsorption groups and storage space. Herein, the activated carbon-hybridized and amine-modified nanofibers are prepared by integrating activated carbon (AC) and polyacrylonitrile (PAN) via electrospinning method and the subsequent amination, which could provide additional storage space and adsorption groups for ultrahigh adsorption capability. Thus, the obtained amine-rich porous PAN nanofibers (APAN/AC) readily realized the ultrahigh adsorption capacity for metal ions and dyes in wastewater. Specifically, the adsorption capacity of APAN/AC nanofibers were 284 mg·g⁻¹ for Cr(VI) and 248 mg·g⁻¹ for methyl orange, which were almost 2 and 4 times than that of amine-modified nanofibers (APAN) and carbon-hybridized nanofibers (PAN/AC), respectively. Moreover, the AC inhibited the chain mobility of polymer matrix and thereby endowing APAN/AC nanofibers with excellent recyclability. The adsorption capability retained 80% after nine adsorption-desorption cycles. The adsorption kinetics and corresponding mechanism were further explored. This strategy combines the advantages of polymer nanofibers and AC, opening a new avenue for developing next-generation absorbent materials.

Keywords carbon-hybridized and amine-modified nanofibers, polyacrylonitrile, metal ions and dyes, wastewater, adsorption kinetics

1 Introduction

Heavy metal wastewater and dye wastewater are two types of water pollution that are environmentally hazardous and difficult to treat. Adsorption method has triggered tremendous attention in wastewater purification, exhaust deodorization and energy recovery due to the feasibility in technology, economy and operation stability [1–7]. Specific surface area, hydrophilic/hydrophobic properties and surface charge are three of the influencing factors that determine the adsorption performance of adsorbents in wastewater treatment [8–10]. Furthermore, the recyclability of adsorbents is another vital consideration in practical application [11–13]. Recently, polymeric nanofibers with excellent recyclability have received great attention among various adsorbents, especially, the polyacrylonitrile (PAN) nanofibers, which have a large specific surface area, strong acid and alkali resistance and excellent mechanical flexibility [14]. It has great application prospects as a kind of recyclable adsorbents [15,16]. In addition, the abundant nitrile groups (C≡N) of PAN nanofibers can participate in targeted chemical reactions to anchor specific adsorption groups [17]. Moreover, it can be easily woven into various shapes for the use in continuous-flow processes [18]. However, due to the lack of the interaction force, PAN nanofibers are usually difficult to adsorb the adsorbates and thus the adsorption capacity of pure PAN nanofibers is negligible [19].

The accessibility of PAN nanofibers can be effectively enhanced by modifying the nanofibers with adsorption groups, thereby generating electrostatic attraction to selectively and fast adsorb the adsorbates [20]. Amine group is one of the adsorption groups exhibiting high binding ability to many metal ions and anionic compounds [21,22]. Chen and co-workers prepared aminated PAN

Received April 20, 2020; accepted July 28, 2020

E-mails: zglcumt@126.com (Zhou G);

zhanglianbi@zzu.edu.cn (Zhang J)

nanofibers by coating polyethyleneimine, whose adsorption capacity to Cu(II) was $149.8 \text{ mg} \cdot \text{g}^{-1}$, higher than that of the pure PAN nanofibers [3]. Furthermore, their study showed that aminated PAN nanofibers exhibited excellent selectivity, and the covalent bonds ensured high adsorption capability and operation stability. The adsorption process mainly occurs on the surface of nanofibers, therefore although many attempts have been made to develop novel functionalized PAN nanofibers, these nanofibers also show unsatisfactory adsorption capacity [23]. Besides, nanofibers with high modifying rate, that is for high adsorption capacity usually do not have excellent mechanical stability due to the enhanced chain mobility and solvent swelling [24]. Thus, nanofibers with extra storage space as well as excellent mechanical stability need to be developed to improve the adsorption performance.

Different from polymeric adsorbents, inorganic materials with porous structure can provide physical space for high-loading adsorption [25–27]. Activated carbon (AC) with high specific surface area and large pore volume is one of the most commonly used inorganic materials [28–30]. However, it has some limitations such as inferior cycle regeneration and poor selectivity, which not only disadvantage the improvement of adsorption performance, but also restrict its practical application [31]. By comparison, if porous nanofibers could be manufactured by integrating polymeric matrix and inorganic AC, they would be promising for significantly improving the adsorption performance through the synergistic effect of these two components. Accordingly, the hybridization of inorganic fillers into polymer matrix via electrospinning method could be an attractive strategy. In this manner, inorganic materials can provide more adsorption sites by creating additional storage space inside the nanofibers, and also inhibit the movement of the polymer chain segments of the high modifying rate nanofibers, thereby enhancing the mechanical stability of polymer nanofibers [32,33]. In addition, the porous hybrid nanofibers prepared by electrospinning method would have some intrinsic advantages including high porosity, large specific surface area and flexibility [34], which is unmatched by traditional casting method. While this kind of porous hybrid nanofibers have rarely reported as adsorbents until now.

Herein, activated carbon-hybridized and amine-modified PAN nanofibers were designed and synthesized by electrospinning PAN and AC, followed by an amination treatment. Synthesized by this way, the storage space inside the nanofibers and the adsorption groups on the surface were significantly improved, as well as the chain mobility was further effectively inhibited. The microstructures and physicochemical properties of these nanofibers were investigated in detail. The adsorption behavior was systematically evaluated by the adsorption isotherms model and adsorption kinetics model. The results showed that the synergistic adsorption effect of electrostatic

attraction and extra storage space of AC made this novel adsorbent ultrahigh adsorption capacity, significantly improved adsorption rate and excellent recyclability. Its adsorption performance for metal ions and dyes ($> 248 \text{ mg} \cdot \text{g}^{-1}$) ranked the highest among PAN nanofibers adsorbents and AC adsorbents. This rationally designed hybrid porous adsorbent which combines the advantages of polymeric nanofibers and porous AC, opens an avenue for high-performance adsorption and separation materials.

2 Experimental

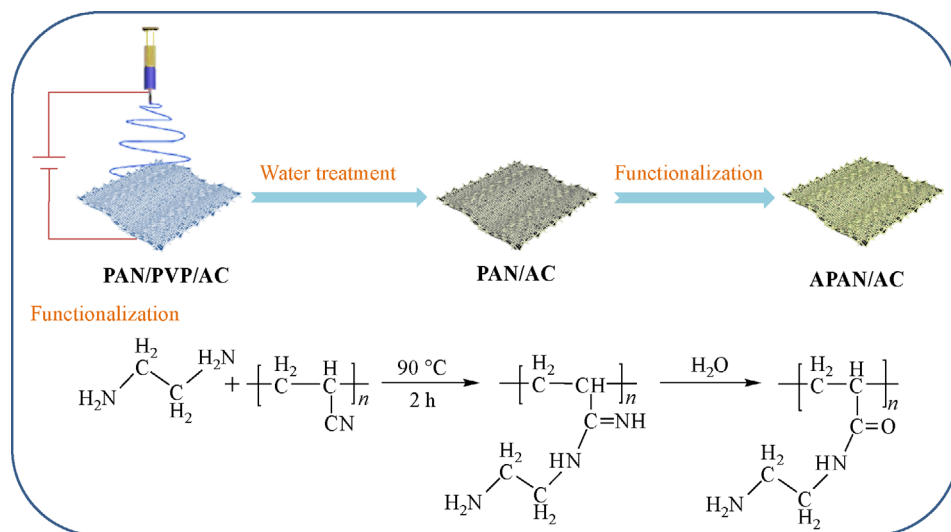
2.1 Materials

PAN ($M_w = 50000 \text{ Da}$) was obtained from Xiamen Feieryang Environmental Protection Co. Ltd. (China). AC was supplied by Laiyang Shuangshuang Chemical Co. Ltd. (China) and it was crushed 1 h under a cell ultrasonic pulverizer (particle size ranges from 40 to 130 nm). Polyvinylpyrrolidone (PVP, $M_w = 1300000 \text{ Da}$), $\text{K}_2\text{Cr}_2\text{O}_7$, and methyl orange (MO) were ordered from Shanghai Aladdin Biochemical Technology Co. Ltd. (China). *N,N*-dimethylformamide (DMF) and ethylenediamine (EDA) were provided by Tianjin Kemiou Chemical Reagent Co. Ltd. (China). The inorganic salt was purchased from Beijing Chemical Factory (China). All other reagents were of analytical grade and used without further purification.

2.2 Synthesis and characterization of APAN/AC nanofibers

2.2.1 Synthesis of APAN/AC nanofibers

A certain mass of AC (Table S1, cf. Electronic Supplementary Material, ESM) was dispersed into DMF (10.0 mL) solution and then ultrasonic treated for 1 h at room temperature. Afterward, PAN (0.75 g) and PVP (0.75 g) were dissolved in the above solution and stirred vigorously for another 12 h. The obtained mixture was fed into a syringe with 0.8 mm needle. An 18 kV voltage was applied on the needle tip, and the collector is kept at a distance of 15 cm to obtain the nanofibers and named as PAN/PVP/AC nanofibers. The above PAN/PVP/AC nanofibers (with an average weight of 0.4 g) were treated with deionized water at $90 \text{ }^\circ\text{C}$ for 1 h to remove PVP, which was named as PAN/AC nanofibers. The proportion of remained PVP could be calculated by formula S1. Then the PAN/AC nanofibers were placed into EDA with concentration of 10%, 15%, 20%, 25% and 30% at $90 \text{ }^\circ\text{C}$ for 2 h and named as APAN/AC nanofibers (Scheme 1). Finally, the obtained nanofibers were washed with water until neutral and then dried at $60 \text{ }^\circ\text{C}$ in the vacuum for 4 h. PAN nanofibers were also prepared by electrospinning without AC and used as a control in this study.



Scheme 1 Schematic diagram of the whole preparation process for APAN/AC nanofibers.

2.2.2 Characterization

The surface morphology of nanofibers was observed by scanning electron microscope (SEM, Auriga FIB SEM, Zeiss, Germany), atomic force microscopy (AFM, Bruker Dimension FastScan) and transmission electron microscope (TEM, Tecnai G2 F20, FEI, U.S.). The chemical components of nanofibers were determined by X-ray diffractometry (XRD, Bruker D8 Advance ECO), fourier transform infrared spectroscopy (FTIR, Tensor27) and X-ray photoelectron spectroscopy (XPS, AXIS Supra, Kratos, UK). The grafting rate of nanofibers was determined by thermal gravimetric analyzer (TGA, NETZSCH STA 2500) and calculated by formula S2. The pore size distribution and the specific surface area were analyzed by Brunauer-Emmett-Teller and Barret-Joyner-Halenda (BET and BJH, ASAP2460). The contact angles were investigated by a contact angle goniometer (JC2000C Contact Angle Meter, Powereach Co.). The elongation at break was analyzed by Instron Mechanical Tester. The concentration of solution was measured by flame atomic absorption spectrophotometer (AAS, TAS-990). The porosity of the nanofibers was determined by the gravimetric analysis method [17]. The point of zero charge (pH_{pzc}) for nanofibers was determined through the pH-drift method [17].

2.3 Adsorption experiments

The adsorption experiments were performed in a thermostatic shaker with a shaking speed of $150\text{ r}\cdot\text{min}^{-1}$. To investigate the effect of initial pH, 10.0 mg APAN/AC nanofibers was added into 20 mL Cr(VI) or MO solution ($80\text{ mg}\cdot\text{L}^{-1}$) with the pH value from 1 to 6, and then shaken for 4 h at a certain temperature. The pH was adjusted with $0.1\text{ mol}\cdot\text{L}^{-1}$ HCl or $0.1\text{ mol}\cdot\text{L}^{-1}$ NaOH solution. The

adsorption capacity (q_e , $\text{mg}\cdot\text{g}^{-1}$) and removal rate (R , %) of the Cr(VI) and MO were calculated by the following equations (1) and (2), respectively:

$$q_e = \frac{(C_0 - C_e)v}{m}, \quad (1)$$

$$R(\%) = \frac{C_0 - C_e}{C_0} \times 100, \quad (2)$$

where the q_e ($\text{mg}\cdot\text{g}^{-1}$) is adsorption amount at equilibrium time, C_0 and C_e ($\text{mg}\cdot\text{L}^{-1}$) are the concentration of Cr(VI) and MO solution at initial and equilibrium, respectively, v (mL) is the liquid phase volume, and m (mg) is the mass of the adsorbent. Then, 10.0 mg nanofibers was added into 20 mL Cr(VI) or MO solution with the initial concentration ranging from 10 to $300\text{ mg}\cdot\text{L}^{-1}$ for the adsorption isotherm experiments. Langmuir and Freundlich isotherm models were used to fit the adsorption isotherm. The equations can be expressed as (3) and (4), respectively:

$$\frac{C_e}{q_e} = \frac{1}{K_L q_m} + \frac{C_e}{q_m}, \quad (3)$$

$$\ln q_e = \ln K_F + \frac{1}{n} \ln C_e, \quad (4)$$

where the K_L ($\text{L}\cdot\text{mg}^{-1}$) and K_F ($\text{mg}\cdot\text{g}^{-1}$) are the equilibrium Langmuir constant and Freundlich constant, respectively, and n is the heterogeneity factor of the adsorption intensity of the adsorbent. The q_e and q_m are the equilibrium and maximum adsorption amount ($\text{mg}\cdot\text{g}^{-1}$), respectively, and C_e ($\text{mg}\cdot\text{L}^{-1}$) is the concentration of Cr(VI) and MO solution at equilibrium.

The adsorption kinetics experiments were conducted by adding 10.0 mg nanofibers into 50 mL Cr(VI) or MO solution ($60\text{ mg}\cdot\text{L}^{-1}$). The pseudo-first-order adsorption

model, pseudo-second-order adsorption model and Weber-Morris model were used as adsorption kinetic models, the Eqs. were expressed as (5)–(7):

$$\ln(q_e - q_t) = \ln q_e - k_1 t, \quad (5)$$

$$\frac{t}{q_t} = \frac{1}{k_2 q_e^2} + \frac{t}{q_e}, \quad (6)$$

$$q_t = k_3 t^{0.5} + c, \quad (7)$$

where the k_1 (min^{-1}), k_2 ($\text{mg} \cdot \text{g}^{-1} \cdot \text{min}^{-1}$) and k_3 ($\text{mg} \cdot \text{g}^{-1} \cdot \text{min}^{-1}$) are the absorption rate constants of pseudo-first-order, pseudo-second-order and Weber-Morris models, respectively, q_e and q_t are the equilibrium and instant adsorption amount ($\text{mg} \cdot \text{g}^{-1}$), respectively.

The effect of temperature experiments were conducted using the mixture of 10.0 mg nanofibers and 20 mL Cr(VI) or MO solution ($80 \text{ mg} \cdot \text{L}^{-1}$), under 20 °C, 30 °C, 40 °C and 50 °C, respectively. The standard Gibbs free energy change (ΔG^0), standard enthalpy change (ΔH^0), and standard entropy change (ΔS^0) were calculated as Eqs. (8–10):

$$\ln K_d = \frac{\Delta S^0}{R} - \frac{\Delta H^0}{RT}, \quad (8)$$

$$K_d = \frac{q_e(m/v)}{C_e}, \quad (9)$$

$$\Delta G^0 = -RT \ln K_d, \quad (10)$$

where the K_d is the adsorption equilibrium constant, R ($8.314 \text{ J} \cdot \text{mol}^{-1} \cdot \text{K}^{-1}$) is the universal gas constant, and T (K) is the temperature.

3 Results and discussion

3.1 Preparation and characterization of the nanofibers

3.1.1 Optimization of preparation conditions

Amine-rich porous nanofibers were synthesized by integrating AC and PAN via electrospinning method and followed by an amination treatment. It was noted that the optimal mass ratio of the added AC to PAN nanofibers was 0.15:1. Lower ratio failed to effectively increase the porosity of nanofibers (Fig. S1, cf. ESM), while higher ratio hindered nanofibers formation and significantly reduced the grafting rate (Fig. S2, cf. ESM). Thus, nanofibers with the AC-to-PAN ratio of 0.15 were used. The nanofibers were grafted by amine groups through amination treatment. The grafting rate of APAN/AC nanofibers was efficiently regulated by the concentration

of EDA solution. A higher amine density means more adsorption sites, which is propitious to improve adsorption ability. Here, the maximum amine grafting rate was 20.6 wt-% under the EDA concentration of 20 wt-% (Fig. S3, cf. ESM). When the concentration of EDA was over 20 wt-%, the amine grafting of APAN/AC nanofibers was decreased because excessive EDA may corrode PAN nanofibers [35]. In addition, the amine grafting rate of APAN nanofibers was 21.5 wt-%, which was slightly higher than that of the APAN/AC nanofibers under the identical grafting conditions (Fig. S4, cf. ESM). It indicated that the effect of such AC ratio on nanofibers grafting reaction was negligible. It was concluded that the preparation conditions of amine-rich porous nanofibers were the AC ratio of 0.15 and the EDA concentration of 20 wt-%.

3.1.2 Characterization

SEM images show that the average diameter of PAN nanofibers is 236 nm (Fig. 1(b)). The incorporation of AC slightly increased the diameter of APAN/AC nanofibers to 256 nm. In addition, some of the AC particles are observed on the surface of APAN/AC nanofibers shedding of non-compact AC particles caused by washing (Fig. 1(d)). Figure S5 (cf. ESM) is the cross-sectional TEM image of APAN/AC nanofibers with the irregular shape of AC marked in red frame, which indicates that the AC has been incorporated into the nanofibers. AFM results show that the hybridization and ammoniation simultaneously bring an obvious change in surface roughness (R_a), from 102.3 for PAN to 136.5 nm for APAN/AC nanofibers (Figs. 1(e) and 1(f)). The increase in the surface roughness of APAN/AC nanofibers contributes to the adsorption rate by promoting droplet spreading.

The chemical features of nanofibers were analyzed by FTIR spectroscopy (Fig. 2(a) and Fig. S6(a) (cf. ESM)). The peak at 2249 cm^{-1} represents the $\text{C}\equiv\text{N}$ stretching of PAN nanofibers, which appears in all nanofibers. Compared with PAN/PVP/AC nanofibers, the peak at $3300\text{--}3500 \text{ cm}^{-1}$ of PVP becomes negligible in PAN/AC nanofibers, indicating that the PVP has almost disappeared. Furthermore, the residual amide peak ($3300\text{--}3500 \text{ cm}^{-1}$) of PVP remained stable in APAN/AC nanofibers. Moreover, compared with PAN nanofibers, the $\text{C}\equiv\text{N}$ in the PAN/AC nanofibers becomes weaker, which is attributed to the effect of the hybridized AC by hydrogen bonding interaction with PAN nanofibers. The $\text{C}\equiv\text{N}$ of PAN nanofibers are weaker in APAN/AC nanofibers than that in PAN/AC nanofibers. Meanwhile, a new peak related to $\text{N}\text{--H}$ stretching bond of amine groups appears at 1574 cm^{-1} , which demonstrates that amine groups have been successfully grafted onto PAN nanofibers. In addition, XRD patterns were also analyzed (Fig. 2(b) and Fig. S6(b)). All nanofibers patterns show a diffraction peak

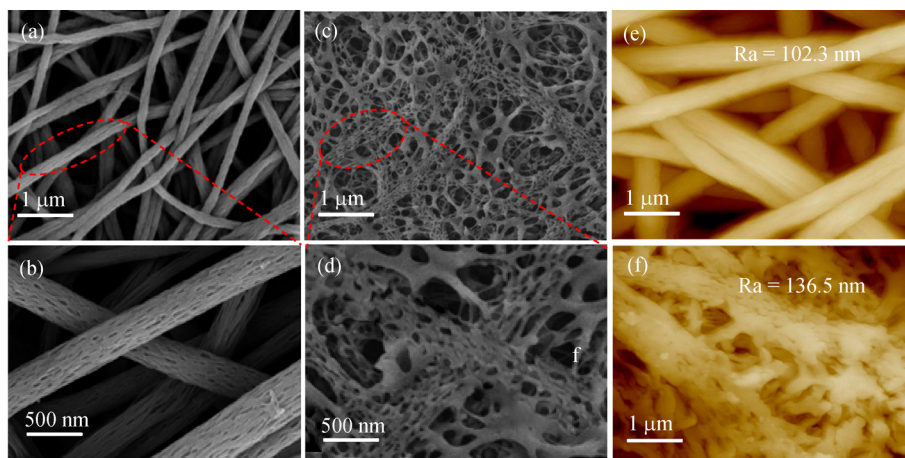


Fig. 1 Surface SEM images of (a), (b) PAN and (c), (d) APAN/AC nanofibers; AFM images of (e) PAN and (f) APAN/AC nanofibers.

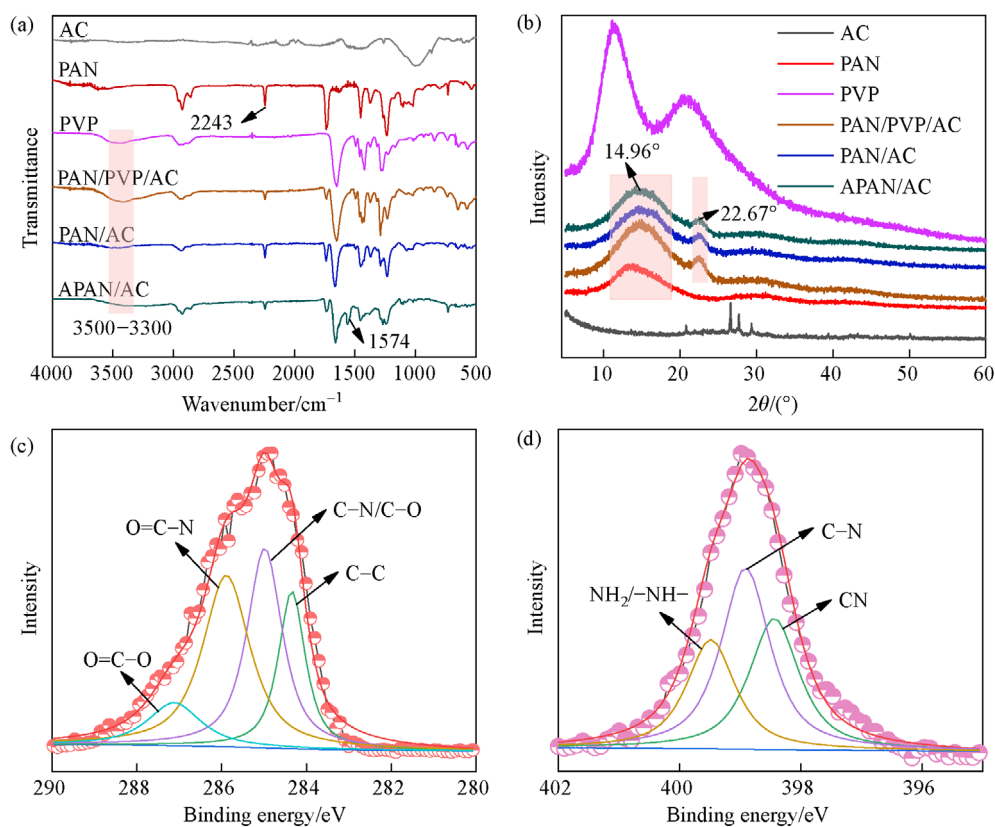


Fig. 2 (a) FTIR pattern and (b) XRD spectra of AC, PVP, PAN, PAN/PVP/AC, PAN/AC and APAN/AC nanofibers, and (c) C 1s and (d) N 1s spectra of APAN/AC nanofibers.

at $2\theta = 14.96^\circ$, corresponding to the (2 0 0) plane of PAN. The crystalline peak of PAN nanofibers and the semi-crystalline peak of PVP ($2\theta = 22.67^\circ$) in PAN/AC nanofibers are significantly weaker than that in PAN/PVP/AC nanofibers, suggesting that most PVP has been removed. Moreover, compared with PAN/AC nanofibers, the variation of crystallization peak strength of APAN/AC nanofibers is negligible, which indicate that the amine

groups have weak effect on the crystallization of nanofibers. The chemical components of APAN/AC nanofibers were further confirmed by XPS. The C 1s spectrum of APAN/AC nanofibers shows four peaks respectively at 284.8, 285.1, 285.9 and 287.2 eV due to C–C, C–N/C–O, O=C–N and O=C–O groups (Fig. 2(c)). The C–N peak of C 1s spectrum suggests the combination of PAN and AC. While the N 1s spectrum forms three

peaks at 398.1, 399.1 and 399.7 eV, corresponding to $C\equiv N$, $N-C$ and $-NH_2/-NH-$, respectively (Fig. 2(d)). The $-NH_2/-NH-$ peak of N 1s spectrum further proves the amination of PAN by EDA.

Elemental analysis of PAN/PVP/AC, PAN/AC and APAN/AC nanofibers were performed and the results were shown in Table 1. The H element content of PAN/AC nanofibers (5.38%) is 1.43% lower than that of the PAN/PVP/AC nanofibers (6.81%), which might be attributed to the removal of PVP. In contrast, the N element content and C/N ratio of APAN/AC nanofibers are increased by 0.63% and dropped by 4.3%, respectively, compared with that of the PAN/AC nanofibers. It indicates that the amine groups have been successfully grafted on the surface of PAN/AC nanofibers.

Table 1 Element analysis results of PAN/PVP/AC, PAN/AC and APAN/AC nanofibers

Samples	N/%	C/%	H/%	C/N
PAN/PVP/AC	15.78	60.99	6.81	3.87
PAN/AC	17.93	61.63	5.38	3.44
APAN/AC	18.56	61.72	6.30	3.33

The pore structure of PAN, PAN/AC and APAN/AC nanofibers was analyzed by BET and shown in Table 2. The specific surface area of APAN/AC nanofibers is $76.2 \text{ m}^2 \cdot \text{g}^{-1}$, which is the highest among these three nanofibers and followed by the PAN and PAN/AC nanofibers with the specific surface area of 32.3 and $68.5 \text{ m}^2 \cdot \text{g}^{-1}$, respectively. Although the diameter of APAN/AC nanofibers is larger than PAN nanofibers, APAN/AC nanofibers have a larger specific surface area, which is different from reported literature [36]. Moreover, the change in pore volume is consistent with the specific surface area. Such phenomenon might be because of the rich porous structures inside APAN/AC nanofibers created by porous AC. The pore feature of PAN, PAN/AC and APAN/AC nanofibers was analyzed by N_2 adsorption/desorption isotherms as depicted in Fig. 3(a). The adsorbed volume is relatively high in the p/p_0 range of 0.7–1.0, the high hysteresis loop indicating the presence of mesoporous structure in nanofibers [10]. As shown in Fig. 3(b), the introduction of AC significantly increases the mesoporous of the PAN/AC and APAN/AC nanofibers, ranging from 10 to 50 nm, as compared to the PAN nanofibers. Such phenomenon demonstrates that AC creates additional mesoporous structure. The vast porous structure would benefit the mass diffusion and adsorption capacity, which is a critical advantage over the traditional nanofibers.

Another key factor of adsorbents is the hydrophilic/hydrophobic property. The contact angle of AC, PAN, APAN and APAN/AC nanofibers was measured. As a typical material with high surface area and porosity, the contact angle of AC reached 2.6° when contacting with the

Table 2 Specific surface area and pore volume of PAN, PAN/AC and APAN/AC nanofibers

Samples	Specific surface area/ $(\text{m}^2 \cdot \text{g}^{-1})$	Pore volume/ $(\text{cm}^3 \cdot \text{g}^{-1})$
PAN	32.3	0.039
PAN/AC	68.5	0.105
APAN/AC	76.2	0.165

water drop instantly (Fig. S7(a), cf. ESM). Figure 3(c) shows the water contact angles of APAN and APAN/AC nanofibers. Their contact angles are approached at initial, but the contact angle of APAN/AC nanofibers is declined visibly faster than that of APAN nanofibers. The final contact angles of APAN and APAN/AC nanofibers are 41.3° and 3.2° , respectively, while that of the PAN nanofibers is 65.3° (Fig. S7(b)). Thus, it could be concluded that the introduction of amine groups increase the hydrophilicity, and the porous AC enhances the molecule diffusion inside the nanofibers. Moreover, the hydrophilicity of the nanofibers was further confirmed by water uptake capacity. The water uptake capacity of APAN/AC nanofibers is 267%, which is much higher than that of APAN nanofibers (166%, Fig. S8, cf. ESM). The highly increased water uptake capacity should be attributed to the porous structure of AC. Collectively, these results imply that APAN/AC nanofibers have the characteristics of high hydrophilicity, water uptake capacity and enhanced molecule diffusion capacity, which would increase the contact of wastewater and further benefit the adsorption of metal ions and dyes.

The structure stability of APAN/AC nanofibers was explored in terms of tensile strain, Young's modulus and swelling degree. Figure S9(a) (cf. ESM) shows that the tensile strain of APAN/AC nanofibers is lower than that of APAN nanofibers, which is consistent with the general trend of nanofiller-doped polymers [37]. On the contrary, the Young's modulus of APAN nanofibers is 16.6 MPa, lower than that of APAN/AC nanofibers (75.0 MPa, Fig. S9(b)), indicating the mechanical properties of nanofibers could be enhanced by compositing AC. Besides, under the identical ammoniating condition, the swelling degree of APAN nanofibers is higher than that of APAN/AC nanofibers (Figs. S10 and S11, cf. ESM). This is because the AC in the PAN polymer matrix inhibits PAN chains mobility and thus limits the swelling degree of nanofibers. The enhanced of nanofibers structure stability guarantees the possibility of long-term operation stability.

3.2 Adsorption performances of nanofibers

3.2.1 Effect of initial pH

The pH value is an important factor affecting adsorption. To explore its influence, this study investigated the adsorption of Cr(VI) and MO by APAN/AC nanofibers with a pH ranging from 1.0 to 6.0. The initial pH of

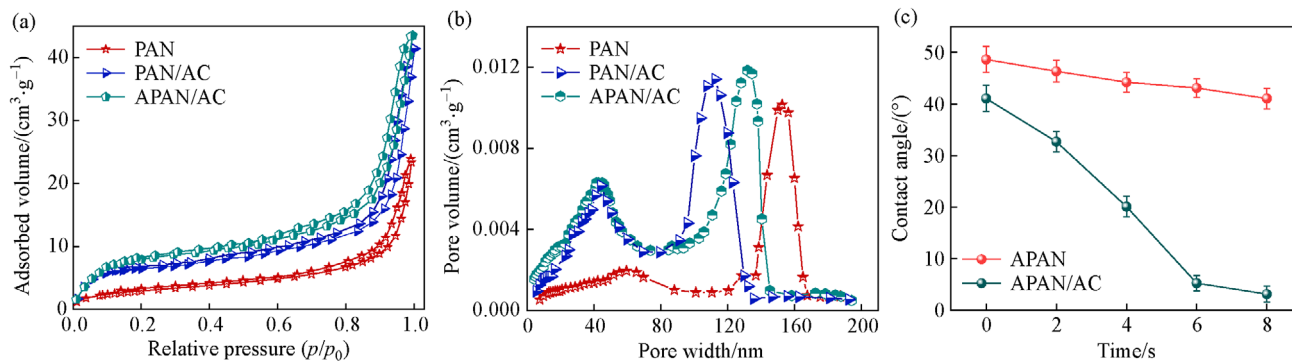


Fig. 3 (a) N_2 adsorption/desorption isotherm and (b) pore size distribution of PAN, PAN/AC and APAN/AC nanofibers, and (c) the water contact angles of APAN and APAN/AC nanofibers.

aqueous solution plays a key role in adsorption due to its influence on the surface properties of adsorbent and the ionization/dissociation of adsorbate molecule. It has been reported in the literature that HCrO_4^- and $\text{Cr}_2\text{O}_7^{2-}$ are predominant of Cr(VI) in the pH range of 2.0–6.0. MO has two chemical structures and its chromophores of anthraquinone and azo bond are altered depending on solution pH (Fig. S12, cf. ESM). To better understand the adsorption process of surface charge of the APAN/AC nanofibers, pH_{pzc} of PAN/AC and APAN/AC nanofibers were measured. The pH_{pzc} of APAN/AC nanofibers is 7.23, which is much higher than 3.26, the pH_{pzc} of PAN/AC nanofibers, suggesting a high positive surface charge is generated due to the grafted amine groups (Fig. 4(a)). The positive charge appeared with the protonation of amine groups in a solution of $\text{pH} < \text{pH}_{\text{pzc}}$ [38]. Figure 4(b) shows the adsorption capacity first increased and then decreased with the increase of pH, and reaches maximum value at $\text{pH} = 3.0$. These results can be explained that positive charges exert strong electrostatic attractions to Cr(VI) and MO [39]. Concretely, the HCrO_4^- and $\text{Cr}_2\text{O}_7^{2-}$ of Cr(VI) and the sulfonic group of MO interact with the protonated amine groups of nanofibers by the electrostatic interaction.

However, the adsorption capacity gradually decreased when the pH is lower than 3.0, because the oxidation of chromate solution becomes strong and easily participates in the redox reactions with other substances. Nevertheless, the redox process is mainly affected by the pH value and the influence becomes strong in the range of pH 0 to 2.0 [40,41]. Thus, the effect of redox reaction on the stability of APAN/AC nanofibers is limited in our experimental range and the ideal initial pH for Cr(VI) and MO removal is 3.0.

3.2.2 Adsorption isotherms

The adsorption capacity of nanofibers was described by the equilibrium isotherms. Figures 5(a) and 5(b) reveal that the adsorption capacity of nanofibers to Cr(VI) and MO increases with the increase of ions concentration, and then reaches a plateau. The maximum adsorption capacities to Cr(VI) and MO of the APAN/AC nanofibers are 284 and 248 $\text{mg} \cdot \text{g}^{-1}$, respectively. Compared with APAN and PAN/AC nanofibers, the adsorption capacity of APAN/AC nanofibers is enhanced by 2 and 4 times, respectively. It highlighted that the introduction of extra storage space

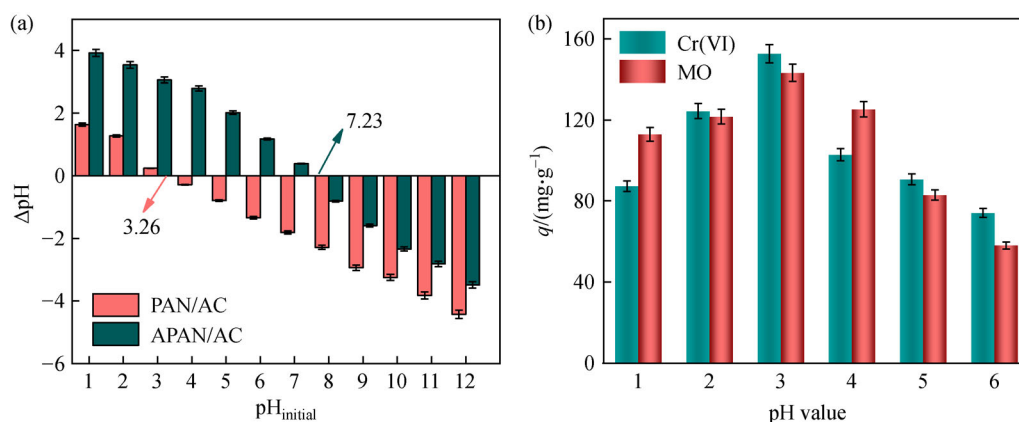


Fig. 4 (a) The ΔpH against $\text{pH}_{\text{initial}}$ plot for PAN/AC and APAN/AC nanofibers, and (b) the adsorption capacity of APAN/AC nanofibers at different pH.

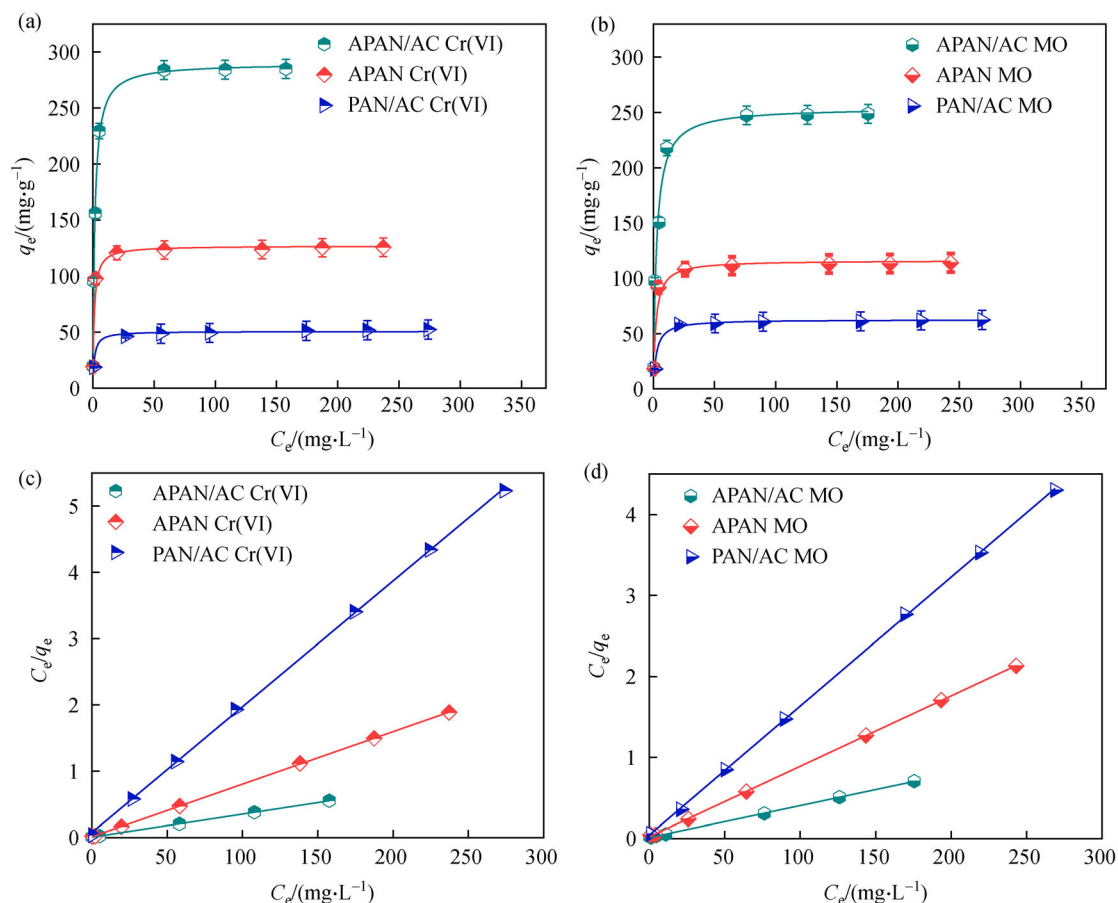


Fig. 5 Adsorption isotherms plots for APAN/AC, APAN, and PAN/AC nanofibers of (a) Cr(VI) and (b) MO, and Langmuir plots of (c) Cr(VI) and (d) MO.

inside nanofibers and adsorption groups on the surface could provide adequate physical space and adsorption sites for ultrahigh adsorption capability. Langmuir model (Figs. 5(c) and 5(d)) and Freundlich model (Figs. S13(a) and S13 (b), cf. ESM) were also used to fit the adsorption results. The corresponding specific parameters and correlation coefficients (R^2) are listed in Table 3. The results indicate that the adsorption plots obey Langmuir model with an R^2 value over 0.99, implying that the adsorption process is more inclined to a monolayer adsorption. Furthermore, the maximum adsorption capacity from the Langmuir model is

quite in agreement with the experimental data. Compared with other reports (Tables S2 and S3, cf. ESM), the present study achieved better adsorption capacity for Cr(VI) and MO, proving the superiority of these amine-rich porous nanofibers.

3.3 Adsorption kinetics

In order to demonstrate the enhancement of adsorption rate of APAN/AC nanofibers, the adsorption kinetics of nanofibers to Cr(VI) and MO were investigated and the

Table 3 Adsorption isotherms parameters for APAN, PAN/AC and APAN/AC nanofibers

Adsorbate		Langmuir isotherm			Freundlich isotherm		
		$q_{cal}/(\text{mg}\cdot\text{g}^{-1})$	$K_L/(\text{L}\cdot\text{mg}^{-1})$	R^2	K_F	n	R^2
APAN	Cr(VI)	126	0.71	0.9993	43.35	4.29	0.6068
	MO	115	0.43	0.9997	34.32	3.89	0.6063
PAN/AC	Cr(VI)	53	0.26	0.9997	21.91	3.15	0.8993
	MO	63	0.37	0.9992	21.79	2.98	0.7951
APAN/AC	Cr(VI)	288	0.62	0.9995	78.07	5.79	0.6889
	MO	254	0.36	0.9996	59.34	4.63	0.6793

results were shown in Figs. 6(a) and 6(b). All the adsorption processes shows two stages: the rapid adsorption at the beginning and the followed slow adsorption stage until adsorption reaches equilibrium. To gain a comprehension of the kinetics and the kinetic mechanism, the pseudo-first-order (Figs. S14(a) and 14(b), cf. ESM) and pseudo-second-order (Figs. 6(c) and 6(d)) models were used to model the kinetic data. The related kinetic parameters are listed in Table 4. The correlation coefficient (R^2) suggest that all the adsorption data are better described by the pseudo-second-order kinetic model [42]. Moreover, the order of adsorption rate is APAN/AC > APAN > PAN/AC nanofibers. These results suggest that the predominant mechanism is based on the electrostatic interaction of amine groups. Furthermore, the adsorption rate of APAN/AC nanofibers is faster, almost 2 times of the APAN nanofibers, which infers that the vast porous structure would benefit to the diffusion of metal ions and dyes, thereby significantly increasing the adsorption rate of APAN/AC nanofibers. The weber-morris model was employed to further evaluate the diffusion mechanism. Figures 6(e) and 6(f) clearly show that the adsorption processes can be divided into two stages. In the first stage, the metal ions and dyes move toward the surface of nanofibers and the adsorption rate is faster. In the second stage, the fitted curves exhibit a comparatively low slope and tend to be flat in virtue of the decrease of available active sites. Neither of the lines pass through the

origin, suggesting that both amine groups and porous structure affect the adsorption rate of APAN/AC nanofibers.

3.4 Thermodynamic evaluation of adsorption

The interaction between nanofibers and adsorbates can be sufficiently explained by ΔG^0 , ΔH^0 and ΔS^0 . The thermodynamic values were calculated from Fig. S15 (cf. ESM). The corresponding parameters of nanofibers are listed in Table 5 and Table S4 (cf. ESM). Negative values of ΔG^0 and positive values of ΔS^0 prove that the adsorption is a spontaneous process. Positive values of ΔH^0 provide the evidence for the endothermic process. Therefore, higher reaction temperature is beneficial for the adsorption process. Generally, the value of ΔH^0 ranged from 2.1 to 20.9 $\text{kJ}\cdot\text{mol}^{-1}$, and 80 to 200 $\text{kJ}\cdot\text{mol}^{-1}$ represent physical and chemical adsorption process, respectively [43]. The ΔH^0 values indicate that chemisorption process occurs on APAN nanofibers (81.89, 89.90 $\text{kJ}\cdot\text{mol}^{-1}$) and physical adsorption process on PAN/AC nanofibers (2.18, 2.43 $\text{kJ}\cdot\text{mol}^{-1}$). By comparison, the ΔH^0 values of APAN/AC nanofibers to Cr(VI) and MO are 54.76 and 61.69 $\text{kJ}\cdot\text{mol}^{-1}$, respectively, which are closer to the realm of physicochemical adsorption. This corresponds to its structure: one part of the metal ions and dyes is bind to amine groups by chemisorption, and the other part enters the AC by physical adsorption.

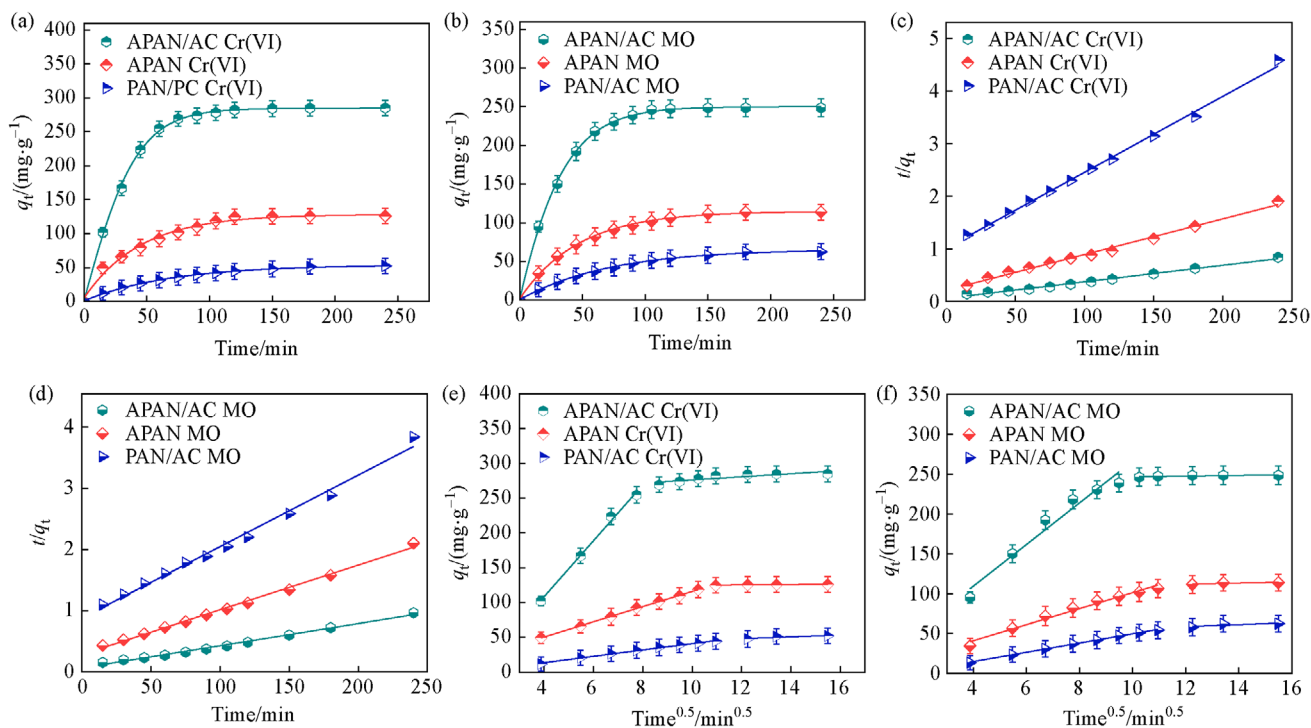


Fig. 6 Adsorption kinetics plots for APAN/AC, APAN, and PAN/AC nanofibers of (a) Cr(VI) and (b) MO, pseudo-second-order kinetic plots of (c) Cr(VI) and (d) MO, and Weber–Morris kinetics plots of (e) Cr(VI) and (f) MO.

Table 4 Adsorption kinetics parameters for APAN, PAN/AC and APAN/AC nanofibers

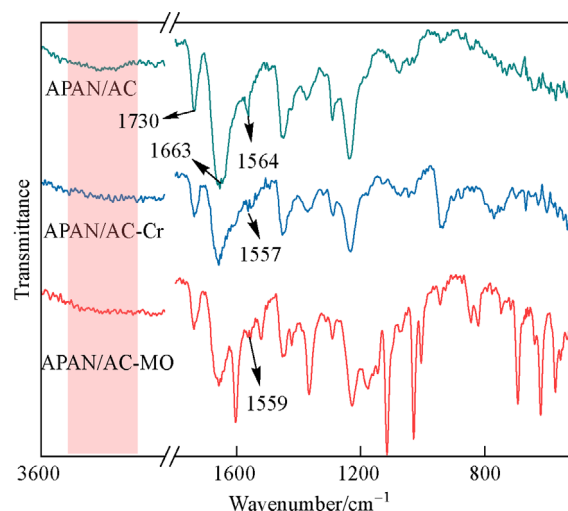
Adsorbate		Pseudo-first-order model		Pseudo-second-order model		Weber–Morris model			
		K_1	R^2	K_2	R^2	$K_{3,1}$	R^2	$K_{3,2}$	R^2
APAN	Cr(VI)	0.029	0.8271	2.03×10^{-4}	0.9913	10.89	0.9935	0.25	0.9905
	MO	0.036	0.6495	1.86×10^{-4}	0.9937	10.02	0.9628	0.63	0.9802
PAN/AC	Cr(VI)	0.029	0.7317	1.53×10^{-4}	0.9926	4.57	0.9998	1.31	0.9956
	MO	0.026	0.7596	1.56×10^{-4}	0.9951	5.81	0.9803	1.23	0.9939
APAN/AC	Cr(VI)	0.018	0.9455	2.13×10^{-4}	0.9973	40.21	0.9945	2.23	0.9605
	MO	0.023	0.7549	1.87×10^{-4}	0.9916	26.12	0.9987	0.41	0.9963

Table 5 The thermodynamic parameters of APAN/AC nanofibers

Item	Temperature/K	$\Delta G^0/(\text{kJ} \cdot \text{mol}^{-1})$	$\Delta H^0/(\text{kJ} \cdot \text{mol}^{-1})$	$\Delta S^0/(\text{J} \cdot \text{mol}^{-1} \cdot \text{K}^{-1})$
Cr(VI)	293	-4.45	54.76	202.09
	303	-6.47		
	313	-8.49		
	323	-10.51		
MO	293	-4.17	61.69	224.78
	303	-6.42		
	303	-8.67		
	323	-10.92		

3.5 Adsorption mechanism

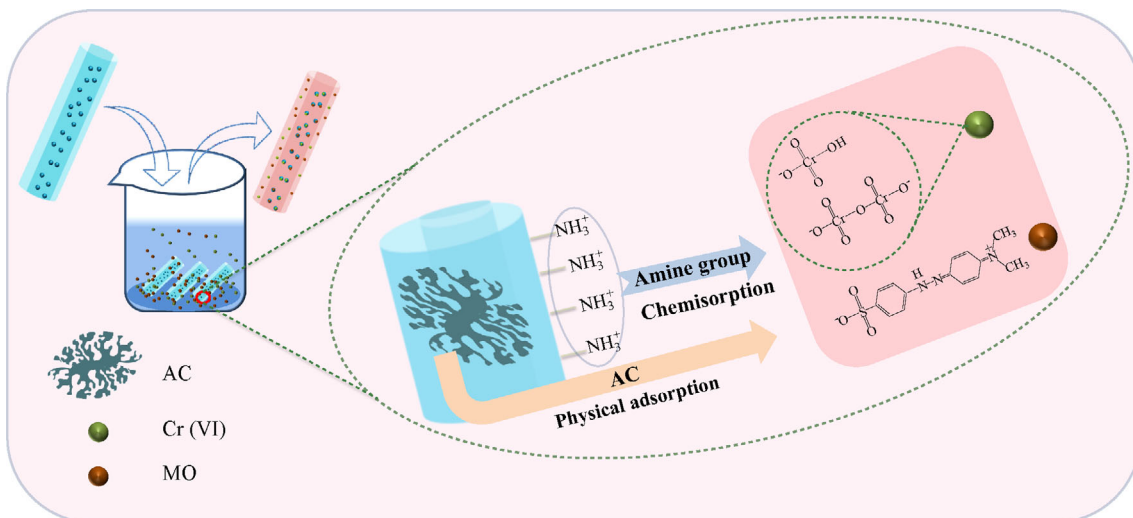
The FTIR analysis was performed before and after the adsorption and was utilized to clarify the adsorption mechanism (Fig. 7). The broad-band ranging of 3300–3500 cm^{-1} corresponds to the overlapping bands of –OH and the stretching vibration of N–H groups. It exhibits the intensity is decreased after adsorbing Cr(VI) or MO, implying the hydrogen-bonding interaction between the adsorbent and adsorbate. Moreover, the bending vibration band of N–H decreased significantly from 1564 to 1557 and 1559 cm^{-1} after adsorbing Cr(VI) and MO, respectively. The band shift and intensity weakness together suggest that the N–H of APAN/AC nanofibers plays an important role in the electrostatic interaction which make the surface of adsorbent positively charged. Compared with APAN/AC nanofibers, the peak strength of C=O at 1730 and 1663 cm^{-1} of PAN and PVP, got weaker after adsorption. However, the PAN nanofibers and pure PAN nanofibers remained 7.89% PVP had negligible adsorption ability as compared to APAN/AC nanofibers (Fig. S16, cf. ESM)). Thus, the weaker peak intensity should be attributed to the attachment of adsorbed ions on nanofibers, which affects the vibration of C=O peak. The adsorption of AC inside the nanofibers is mainly due to the hydrogen bonding interaction of –OH with the HCrO_4^- and $\text{Cr}_2\text{O}_7^{2-}$ of Cr(VI) or the sulfonic group of MO. The aforementioned analyses demonstrate that the force between the adsorbent and the adsorbate in the adsorption process is

**Fig. 7** FTIR spectra of pure APAN/AC nanofibers and after adsorption.

mainly the electrostatic interaction and hydrogen-bonding interaction. Furthermore, the adsorption mechanism of the APAN/AC nanofibers includes the synergistic interaction with amine groups and AC, corresponding to the aforementioned analyses (Scheme 2).

3.6 Effect of coexisting anions and adsorption cycles

There are multiple anions existing in natural polluted waters, which could reduce the adsorption efficiency of



Scheme 2 Schematic illustration of APAN/AC nanofibers for Cr(VI) and MO adsorption in wastewater.

APAN/AC nanofibers. Thus, it is necessary to study the effect of coexisting anions, and Cl^- , SO_4^{2-} and NO_3^- are chosen as the representative competition anions [44]. The concentration of the anions used in the experiment was $10 \text{ mmol}\cdot\text{L}^{-1}$ and the concentration of Cr(VI) or MO was $80 \text{ mg}\cdot\text{L}^{-1}$. Figure 8(a) shows that these ions have little effect on adsorption capacity. In comparison, the effect of SO_4^{2-} is higher than Cl^- and NO_3^- . The different attractions of APAN/AC nanofibers toward ions mainly depend on the ion charge density [45].

To assess the reusability of APAN/AC nanofibers, adsorption-desorption recycling to Cr(VI) and MO was performed (Fig. 8(b)). The cyclic experiments show that the adsorption capacity of APAN/AC nanofibers to Cr(VI) and MO remains at 88% and 82% after nine cycles, respectively. The mass loss of APAN/AC nanofibers is only 11% (Fig. S17, cf. ESM) and the characteristic absorption peaks of recycled APAN/AC nanofibers change slightly (Fig. S18, cf. ESM). The shedding of AC is the

main cause of the mass loss of APAN/AC nanofibers. The minor-change of characteristic adsorption peaks might be because of the destruction of functional groups during the cycling experiment. The above reasons collectively lead to the decrease of adsorption performance. For a further research, the APAN/AC nanofibers were soaked in acidic, alkaline, saline and DMF solutions for 7 d. As shown in Fig. S19 (cf. ESM), the nanofibers show a stable structure and maintain integrated structure except for being dissolved in DMF. All these results suggest that the APAN/AC nanofibers possess excellent physical and chemical stabilities, solvent resistance and reusability, and have great promise as a recyclable adsorbent for wastewater treatment.

4 Conclusions

In summary, the amine-rich porous nanofibers were

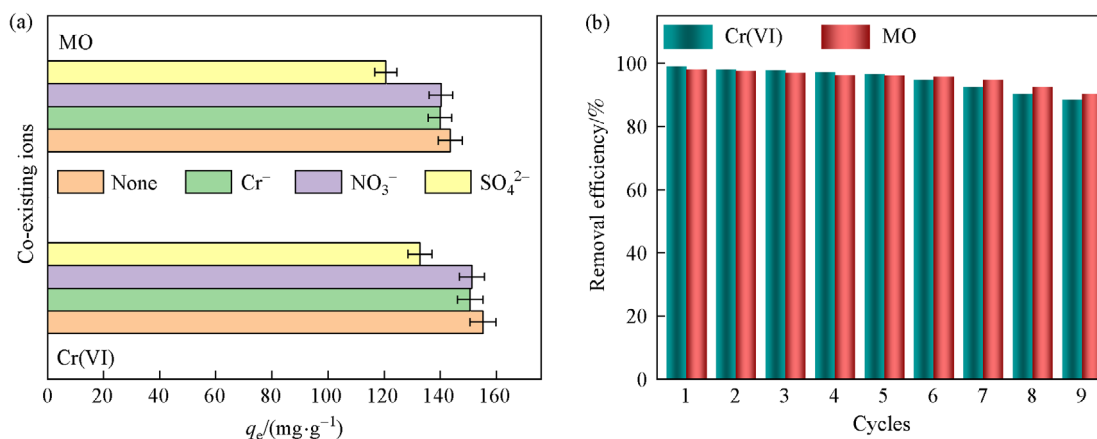


Fig. 8 (a) Effect of coexisting ions and (b) regeneration cycle study.

developed successfully by integrating AC and PAN via electrospinning method and a followed amination treatment. Grafting amine groups on the surface of nanofibers endow APAN/AC nanofibers with electrostatic interactions, high hydrophilicity and abundant surface adsorption sites. In addition, the AC inside nanofibers endows APAN/AC nanofibers additional storage space, enhanced mechanical stability and molecule diffusion inside the nanofibers. The adsorption process of APAN/AC nanofibers obeys Langmuir adsorption and readily realizes ultrahigh adsorption capacity of $284 \text{ mg} \cdot \text{g}^{-1}$ for Cr(VI) and $248 \text{ mg} \cdot \text{g}^{-1}$ for MO, which is higher than most of the reported nanofiber-based adsorbents. In addition, APAN/AC nanofibers exhibit a rapid adsorption rate due to the electrostatic interaction of amine groups, which plays a crucial role in the adsorption process. Moreover, the vast porous structure further promotes the adsorption rate. The adsorption thermodynamic of APAN/AC nanofibers is close to the realm of physicochemical adsorption due to the amine-rich porous structure. Furthermore, the nanofibers show excellent reusability and can maintain 80% adsorption capacity after nine cycles. Considering the low cost of AC and PAN, ease of industrial preparation, excellent reusability and high adsorption capacity, the nanofibers developed in this study might be a promising material in the field of wastewater treatment.

Acknowledgements This work is supported by Natural Science Foundation of Henan Province (Grant No. 182300410276), the National Natural Science Foundation of China (Grant No. 51904274) and Program for Innovative Research Team (in Science and Technology) in University of Henan Province (Grant No. 19IRTSTHN028).

Electronic Supplementary Material Supplementary material is available in the online version of this article at <https://doi.org/10.1007/s11705-020-2000-3> and is accessible for authorized users.

References

- Tian L, Jiang H, Chen P, Wang Q, Niu P, Shi Y, Zhou M, Qing Y, Luo X. A novel GO/PNIPAm hybrid with two functional domains can simultaneously effectively adsorb and recover valuable organic and inorganic resources. *Chemical Engineering Journal*, 2018, 343: 607–618
- Yu J, Zhu S, Chen P, Zhu G T, Jiang X, Di S. Adsorption behavior and mechanism of Pb(II) on a novel and effective porphyrin-based magnetic nanocomposite. *Applied Surface Science*, 2019, 484: 124–134
- Chen C, Li F, Guo Z, Qu X, Wang J, Zhang J. Preparation and performance of aminated polyacrylonitrile nanofibers for highly efficient copper ion removal. *Colloids and Surfaces. A, Physicochemical and Engineering Aspects*, 2019, 568: 334–344
- Wang J, Yi H, Tang X, Zhao S, Gao F. Simultaneous removal of SO_2 and NO_x by catalytic adsorption using $\gamma\text{-Al}_2\text{O}_3$ under the irradiation of non-thermal plasma: competitiveness, kinetic, and equilibrium. *Chemical Engineering Journal*, 2020, 384: 123334
- Cheng Y, He P, Dong F, Nie X, Ding C, Wang S, Zhang Y, Liu H, Zhou S. Polyamine and amidoxime groups modified bifunctional polyacrylonitrile-based ion exchange fibers for highly efficient extraction of U(VI) from real uranium mine water. *Chemical Engineering Journal*, 2019, 367: 198–207
- Ju P, Liu Q, Zhang H, Chen R, Liu J, Yu J, Liu P, Zhang M, Wang J. Hyperbranched topological swollen-layer constructs of multi-active sites polyacrylonitrile (PAN) adsorbent for uranium(VI) extraction from seawater. *Chemical Engineering Journal*, 2019, 374: 1204–1213
- Zhang L, Zhou D, Yao Q, Zhou J. Preparation of H_2TiO_3 -lithium adsorbent by the sol-gel process and its adsorption performance. *Applied Surface Science*, 2016, 368: 82–87
- Gupta K, Gupta D, Khatri O P. Graphene-like porous carbon nanostructure from bengal gram bean husk and its application for fast and efficient adsorption of organic dyes. *Applied Surface Science*, 2019, 476: 647–657
- Yuan Y, Zhao S, Wen J, Wang D, Guo X, Xu L, Wang X, Wang N. Rational design of porous nanofiber adsorbent by blow-spinning with ultrahigh uranium recovery capacity from seawater. *Advanced Functional Materials*, 2019, 29(2): 1805380
- Zhu Z, Wu P, Liu G, He X, Qi B, Zeng G, Wang W, Sun Y, Cui F. Ultrahigh adsorption capacity of anionic dyes with sharp selectivity through the cationic charged hybrid nanofibrous membranes. *Chemical Engineering Journal*, 2017, 313: 957–966
- Shao Y, Zhou L, Bao C, Ma J, Liu M, Wang F. Magnetic responsive metal-organic frameworks nanosphere with core-shell structure for highly efficient removal of methylene blue. *Chemical Engineering Journal*, 2016, 283: 1127–1136
- Yuan X, Zhou C, Jin Y, Jing Q, Yang Y, Shen X, Tang Q, Mu Y, Du A K. Facile synthesis of 3D porous thermally exfoliated g- C_3N_4 nanosheet with enhanced photocatalytic degradation of organic dye. *Journal of Colloid and Interface Science*, 2016, 468: 211–219
- Liu Y, Xu L, Liu J, Liu X, Chen C, Li G, Meng Y. Graphene oxides cross-linked with hyperbranched polyethylenimines: preparation, characterization and their potential as recyclable and highly efficient adsorption materials for lead(II) ions. *Chemical Engineering Journal*, 2016, 285: 698–708
- Xiao J, Xu G, Wang L, Li P, Zhang W, Ma N, Tao M. Polyacrylonitrile fiber with strongly acidic electrostatic microenvironment: highly efficient and recyclable heterogeneous catalyst for the synthesis of heterocyclic compounds. *Journal of Industrial and Engineering Chemistry*, 2019, 77: 65–75
- Zhu H, Xu G, Du H, Zhang C, Ma N, Zhang W. Prolineamide functionalized polyacrylonitrile fiber with tunable linker length and surface microenvironment as efficient catalyst for Knoevenagel condensation and related multicomponent tandem reactions. *Journal of Catalysis*, 2019, 374: 217–229
- Zheng L, Li P, Tao M, Zhang W. Regulation of polar microenvironment on the surface of tertiary amines functionalized polyacrylonitrile fiber and its effect on catalytic activity in Knoevenagel condensation. *Catalysis Communications*, 2019, 118: 19–24

17. Zhao R, Li X, Sun B, Li Y, Li Y, Yang R, Wang C. Branched polyethylenimine grafted electrospun polyacrylonitrile fiber membrane: a novel and effective adsorbent for Cr(VI) remediation in wastewater. *Journal of Materials Chemistry. A, Materials for Energy and Sustainability*, 2017, 5(3): 1133–1144
18. Dai L, Cui L, Zhou D, Huang J, Yuan S. Resource recovery of Cr (VI) from electroplating wastewater: laboratory and pilot-scale investigation using fibrous weak anion exchanger. *Journal of the Taiwan Institute of Chemical Engineers*, 2015, 54: 170–177
19. Deng S, Wang P, Zhang G, Dou Y. Polyacrylonitrile-based fiber modified with thiosemicarbazide by microwave irradiation and its adsorption behavior for Cd(II) and Pb(II). *Journal of Hazardous Materials*, 2016, 307: 64–72
20. Xiao J, Wang L, Ran J, Zhao J, Tao M, Zhang W. Highly selective removal of cationic dyes from water by acid-base regulated anionic functionalized polyacrylonitrile fiber: fast adsorption, low detection limit, reusability. *Reactive & Functional Polymers*, 2020, 146: 104394
21. Wang B, Chen P Y, Zhao R X, Zhang L, Chen Y, Yu L P. Carbon-dot modified polyacrylonitrile fibers: recyclable materials capable of selectively and reversibly adsorbing small-sized anionic dyes. *Chemical Engineering Journal*, 2019, 391: 123484
22. Liu J, Su D, Yao J, Huang Y, Shao Z, Chen X. Soy protein-based polyethylenimine hydrogel and its high selectivity for copper ion removal in wastewater treatment. *Journal of Materials Chemistry. A, Materials for Energy and Sustainability*, 2017, 5(8): 4163–4171
23. Deng S, Zhang G, Wang X, Zheng T, Wang P. Preparation and performance of polyacrylonitrile fiber functionalized with iminodiacetic acid under microwave irradiation for adsorption of Cu(II) and Hg(II). *Chemical Engineering Journal*, 2015, 276: 349–357
24. Bai H, Li Y, Zhang H, Chen H, Wu W, Wang J, Liu J. Anhydrous proton exchange membranes comprising of chitosan and phosphorylated graphene oxide for elevated temperature fuel cells. *Journal of Membrane Science*, 2015, 495: 48–60
25. Hughes D L, Afsar A, Harwood L M, Jiang T, Laventine D M, Shaw L J, Hodson M E. Adsorption of Pb and Zn from binary metal solutions and in the presence of dissolved organic carbon by DTPA-functionalised, silica-coated magnetic nanoparticles. *Chemosphere*, 2017, 183: 519–527
26. Abdi J, Vossoughi M, Mahmoodi N M, Alemzadeh I. Synthesis of metal-organic framework hybrid nanocomposites based on GO and CNT with high adsorption capacity for dye removal. *Chemical Engineering Journal*, 2017, 326: 1145–1158
27. Chen D, Sun H, Wang Y, Quan H, Ruan Z, Ren Z, Luo X. UiO-66 derived zirconia/porous carbon nanocomposites for efficient removal of carbamazepine and adsorption mechanism. *Applied Surface Science*, 2020, 507: 145054
28. Li X, Yuan H, Quan X, Chen S, You S. Effective adsorption of sulfamethoxazole, bisphenol A and methyl orange on nanoporous carbon derived from metal-organic frameworks. *Journal of Environmental Sciences (China)*, 2018, 63: 250–259
29. Li Y, Qi B, Wan Y. Separation of monosaccharides from pretreatment inhibitors by nanofiltration in lignocellulosic hydrolysate: fouling mitigation by activated carbon adsorption. *Biomass and Bioenergy*, 2020, 136: 105527
30. Onuki S, Koziel J A, Jenks W S, Cai L, Rice S, van Leeuwen J. Ethanol purification with ozonation, activated carbon adsorption, and gas stripping. *Separation and Purification Technology*, 2015, 151: 165–171
31. Guillossou R, Le Roux J, Mailler R, Pereira-Derome C S, Varrault G, Bressy A, Vulliet E, Morlay C, Nauleau F, Rocher V, Gasperi J. Influence of dissolved organic matter on the removal of 12 organic micropollutants from wastewater effluent by powdered activated carbon adsorption. *Water Research*, 2020, 172: 115487
32. Zhao L, Li Y, Zhang H, Wu W, Liu J, Wang J. Constructing proton-conductive highways within an ionomer membrane by embedding sulfonated polymer brush modified graphene oxide. *Journal of Power Sources*, 2015, 286: 445–457
33. Zhang H, He Y, Zhang J, Ma L, Li Y, Wang J. Constructing dual-interfacial proton-conducting pathways in nanofibrous composite membrane for efficient proton transfer. *Journal of Membrane Science*, 2016, 505: 108–118
34. Jones B, Britton J, Mafukidze D, Nyokong T. Photodegradation of 4-chlorophenol using Zn and In phthalocyanines substituted with pyrrole without hetero atoms linkers and supported on polyacrylonitrile electrospun fibres. *Polyhedron*, 2020, 178: 114329
35. Liu Z T, Yang Y, Zhang L, Sun P, Liu Z W, Lu J, Xiong H, Peng Y, Tang S. Study on the performance of ramie fiber modified with ethylenediamine. *Carbohydrate Polymers*, 2008, 71(1): 18–25
36. Neghlani P K, Rafizadeh M, Taromi F A. Preparation of aminated-polyacrylonitrile nanofiber membranes for the adsorption of metal ions: comparison with microfibers. *Journal of Hazardous Materials*, 2011, 186(1): 182–189
37. Yuan Z, Wu X, Jiang Y, Li Y, Huang J, Hao L, Zhang J, Wang J. Carbon dots-incorporated composite membrane towards enhanced organic solvent nanofiltration performance. *Journal of Membrane Science*, 2018, 549: 1–11
38. Bouchoum H, Benmoussa D, Jada A, Tahiri M, Cherkaoui O. Synthesis of amidoximated polyacrylonitrile fibers and its use as adsorbent for Cr(VI) ions removal from aqueous solutions. *Environmental Progress & Sustainable Energy*, 2019, 38(5): 13196
39. Liu X, Tian J, Li Y, Sun N, Mi S, Xie Y, Chen Z. Enhanced dyes adsorption from wastewater via Fe₃O₄ nanoparticles functionalized activated carbon. *Journal of Hazardous Materials*, 2019, 373: 397–407
40. Ma Y, Zhang B, Ma H, Yu M, Li L, Li J. Electrospun nanofibrous polyethylenimine mat: a potential adsorbent for removal of chromate and arsenate from drinking water. *RSC Advances*, 2016, 6(36): 30739–30746
41. Weckhuysen B M, Wachs I E, Schoonheydt R A. Surface chemistry and spectroscopy of chromium in inorganic oxides. *Chemical Reviews*, 1996, 96(8): 3327–3350
42. Chen S, Xie F. Selective adsorption of Copper (II) ions in mixed solution by Fe₃O₄-MnO₂-EDTA magnetic nanoparticles. *Applied Surface Science*, 2020, 507: 145090
43. Jiang X, Xiang X, Peng S, Hou L. Facile preparation of nitrogen-doped activated mesoporous carbon aerogel from chitosan for methyl orange adsorption from aqueous solution. *Cellulose (London, England)*, 2019, 26(7): 4515–4527
44. Li Y, Zhao R, Chao S, Sun B, Wang C, Li X. Polydopamine coating

- assisted synthesis of MnO₂ loaded inorganic/organic composite electrospun fiber adsorbent for efficient removal of Pb²⁺ from water. *Chemical Engineering Journal*, 2018, 344: 277–289
45. Qiu J, Liu F, Cheng S, Zong L, Zhu C, Ling C, Li A. Recyclable nanocomposite of flowerlike MoS₂@Hybrid acid-doped PANI immobilized on porous PAN nanofibers for the efficient removal of Cr(VI). *ACS Sustainable Chemistry & Engineering*, 2018, 6(1): 447–456